Supplementary Information

Molecular Order Manipulation with Dual Additives Suppressing Trap Density in Non-Fullerene Acceptors Enables Efficient Bilayer Organic Solar Cells

Zhenmin Zhao[1], Sein Chung[2], Lixing Tan[1], Jingjing Zhao[1], Yuan Liu [1], Xin Li[1], Liang Bai[1], Hyunji Lee[2], Minyoung Jeong[2], Kilwon Cho[2], Zhipeng Kan[1,3]*

[1] Center on Nanoenergy Research, Institute of Science and Technology for Carbon Peak & Neutrality, School of Physical Science & Technology, Guangxi University, Nanning 530004, China.

[2] Department of Chemical Engineering, Pohang University of Science and Technology, Pohang 37673, South Korea.

[3] State Key Laboratory of Featured Metal Materials and Life-cycle Safety for Composite Structures, Nanning 530004, China.

* Corresponding author, E-mail: kanzhipeng@gxu.edu.cn

Content

1. Experimental Section/Methods

Materials: PM6 and L8-BO were purchased from Dongguan Volt-Amp Optoelectronics Technology Co., Ltd. PEDOT:PSS (CLEVIOSTM P VP AI 4083, Heraeus, Germany) was purchased from Xi'an Yuri Solar Co., Ltd. PDIN was purchased from Organtec Ltd.

Device Fabrication: Bilayer organic solar cells were prepared on glass substrates with tin-doped indium oxide (ITO, 15 Ω/sq) (device area: 0.04 cm2). Substrates were prewashed with isopropanol to remove organic residues before immersing them in an ultrasonic bath of soap for 15 min. Samples were rinsed in flowing deionized water for 5 min before being sonicated for 15 min each in successive baths of deionized water, acetone, and isopropanol. Next, the samples were dried with pressurized nitrogen before being exposed to a UV-ozone plasma for 15 min. A thin layer of PEDOT:PSS (~20 nm) (Clevios AL4083) was spin-coated onto the UV-treated substrates, the PEDOT-coated substrates were subsequently annealed on a hot plate at 150 °C for 20 min, and the substrates were then transferred into the glovebox for active layer deposition.

For the solar cells with a bilayer architecture, PM6 in chloroform solution (8 mg/mL) was bladed on the PEDOT: PSS layer to form a front layer, and then a solution of the L8-BO (10 mg/mL) in dichloromethane (DCM) with or without additives were bladed onto the donor layer. Then, a methanol solution of PDIN at a concentration of 2.0 mg/ml with acetic acid (0.3 vol%) was spin-coated onto the active layer at 5000 rpm. Next, the substrates were pumped down in a high vacuum at a pressure of 3×10^{-4} Pa, and the Ag layer (100 nm) was thermally evaporated onto the PDIN.

Photocurrent measurements: The J−V measurement was performed via a XES-50S1 (SAN-EI Electric Co., Ltd.) solar simulator (AAA grade) whose intensity was calibrated by a certified standard silicon solar cell (SRC-2020, Enlitech) under the illumination of AM 1.5G 100 mW cm^{-2}. The AM 1.5G light source with a spectral mismatch factor of 1.01 was calibrated by the National Institute of Metrology. The intensity of the AM 1.5G spectra was calibrated by a certified standard silicon solar cell

(SRC-2020, Enlitech) calibrated by the National Institute of Metrology. The J-V curves of small-area devices were measured in forwarding scan mode (from -0.2 V to 1.2 V) with a scan step length of 0.02 V. The external quantum efficiency (EQE) was measured by a certified incident photon to electron conversion (IPCE) equipment (QE-R) from Enli Technology Co., Lt. The light intensity at each wavelength was calibrated using a standard monocrystalline Si photovoltaic cell. Optoelectronic characterizations were performed with PAIOS (Fluxim, Switzerland).

2. Energy level of PM6, L8-BO

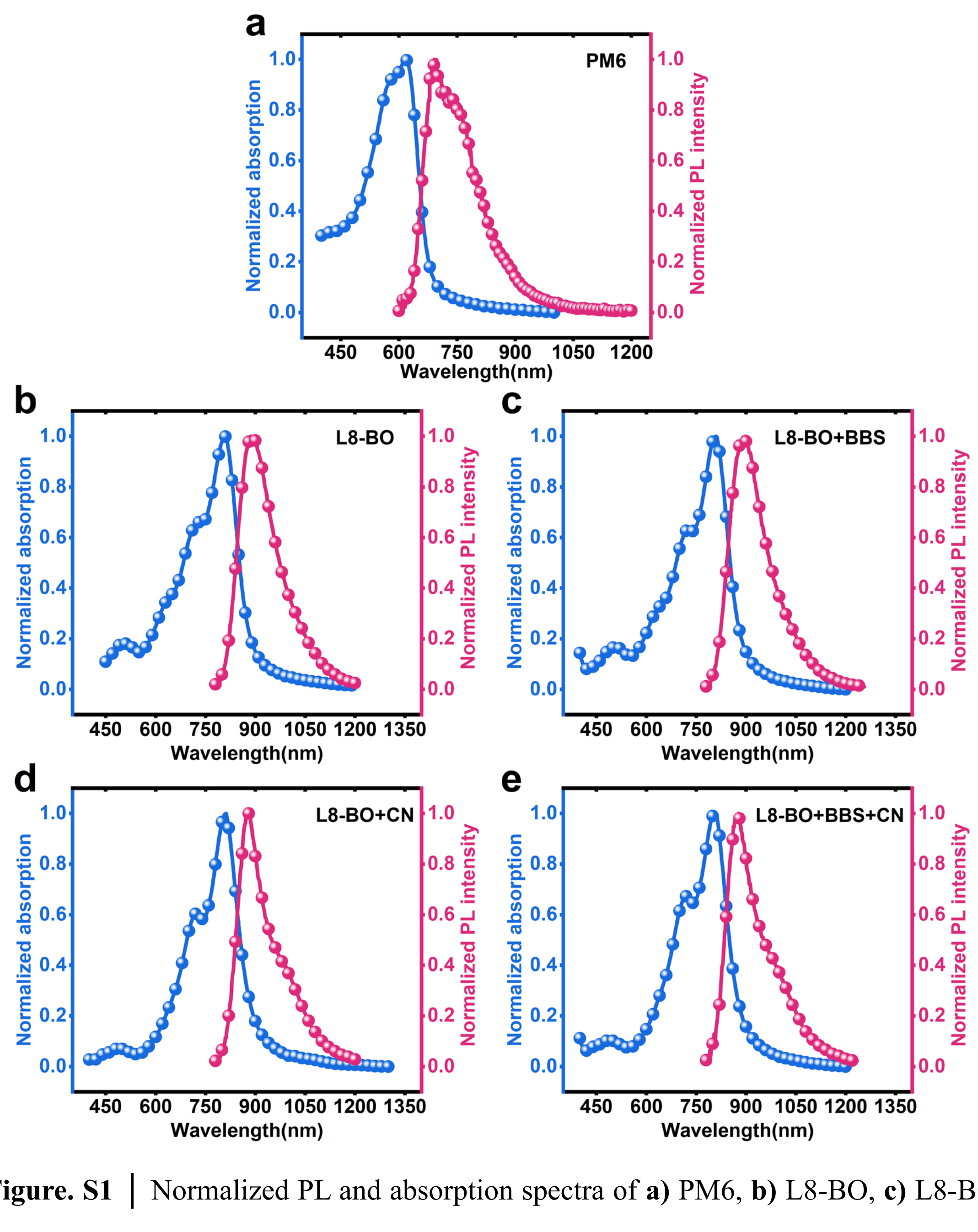

Figure. S1 │ Normalized PL and absorption spectra of **a)** PM6, **b)** L8-BO, **c)** L8-BO with BBS, **d)** L8-BO with CN, **e)** L8-BO with BBS+CN.

3. AFM measurements of L8-BO with and without additives

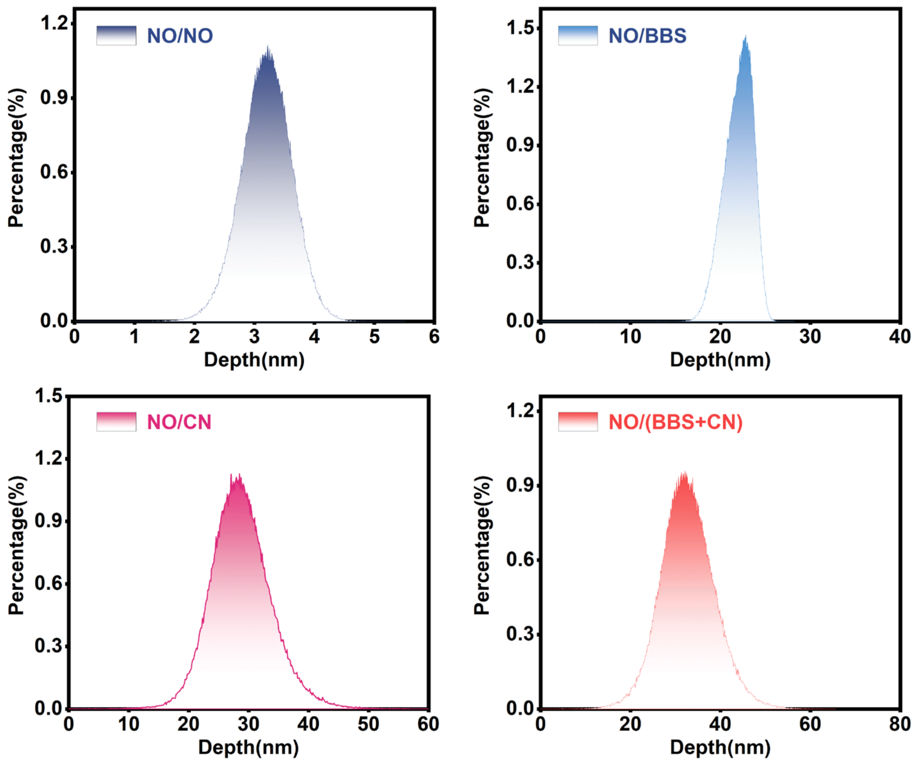

Figure. S2 │ Depth of L8-BO films changed with additives.

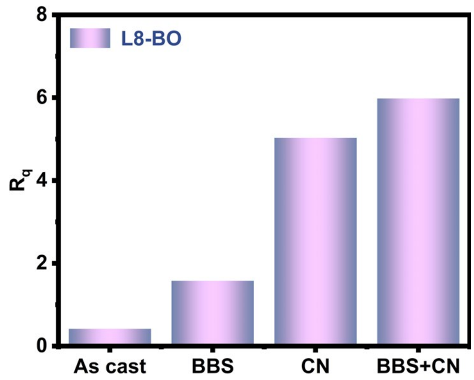

Figure. S3 │ Roughness of L8-BO films changed with additive

4. GIWAXS measurements of L8-BO with and without additives

Grazing-incidence wide-angle X-ray scattering (GIWAXS) was carried out to investigate the molecular packing and molecular orientation in the thin films. The π–π stacking distance (d-spacing) and crystalline coherence length (CCL) were calculated quantitatively using the equations d-spacing = $2\pi/q$ and CCL = $2\pi K/\Delta q$, where q, Δq and the K constant represent the peak positions, full width at half maximum. [1,2]

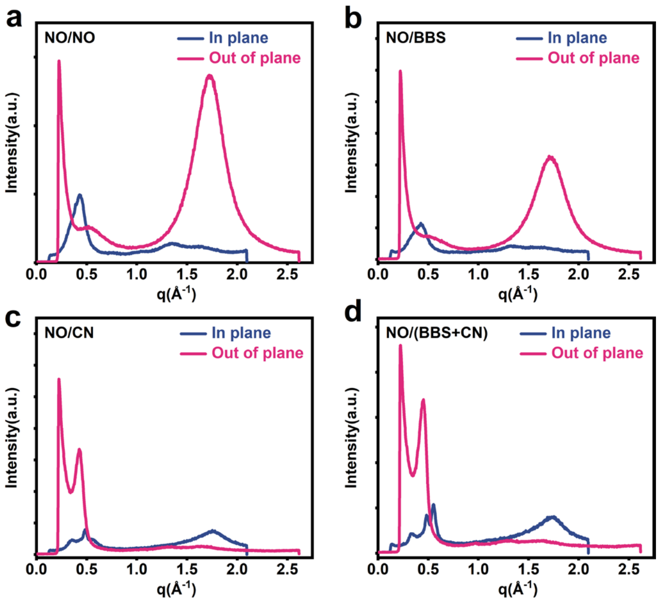

Figure S4. In-plane (dash lines) and out-of-plane (solid lines) line cuts of L8-BO films cast from **a)** DCM, **b)** DCM with BBS, **c)** DCM with CN, and **d)** DCM with BBS+CN.

Table S1 | In-plane and out-of-plane parameters; peak location, d-spacing, FWHM, and crystal coherence length (CCL) extracted from the 2D GIWAXS of L8-BO films with and without additives.

Condition	Peak	Peak location (Å^{-1})	d-space (Å)	FWHM (Å^{-1})	CCL (Å)
As cast	(010)	1.72	3.65	0.30	19.04
BBS	(010)	1.72	3.65	0.31	18.07
CN	(100)	1.74	3.61	0.17	33.26
BBS+CN	(100)	1.73	3.63	0.22	25.70

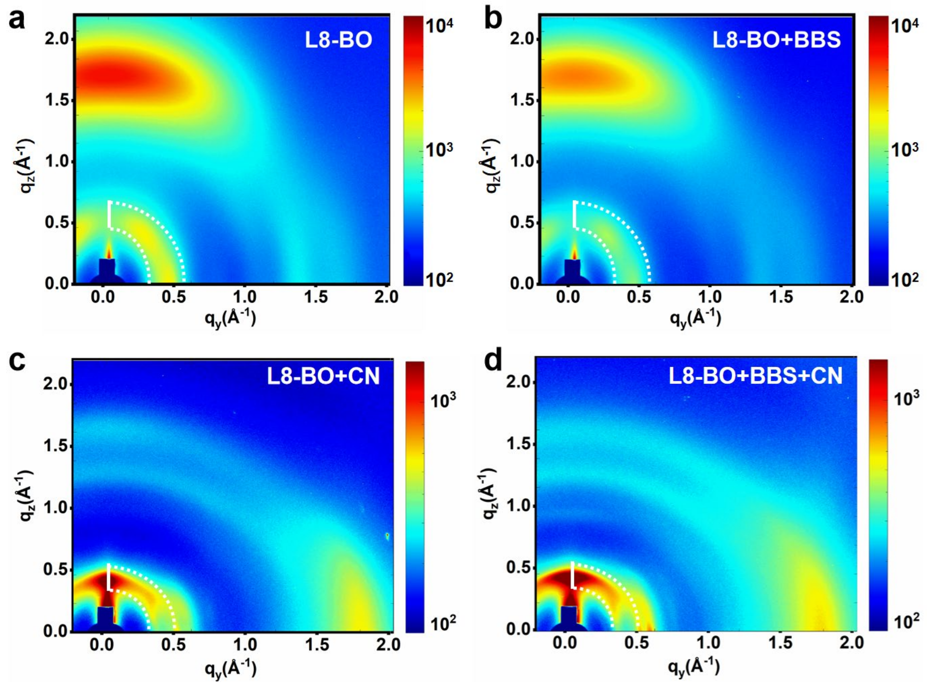

Figure S5. │ 2D-GIWAXS pattern of L8-BO films cast from **a)** DCM, **b)** DCM with BBS, **c)** DCM with CN, and **d)** DCM with BBS+CN.

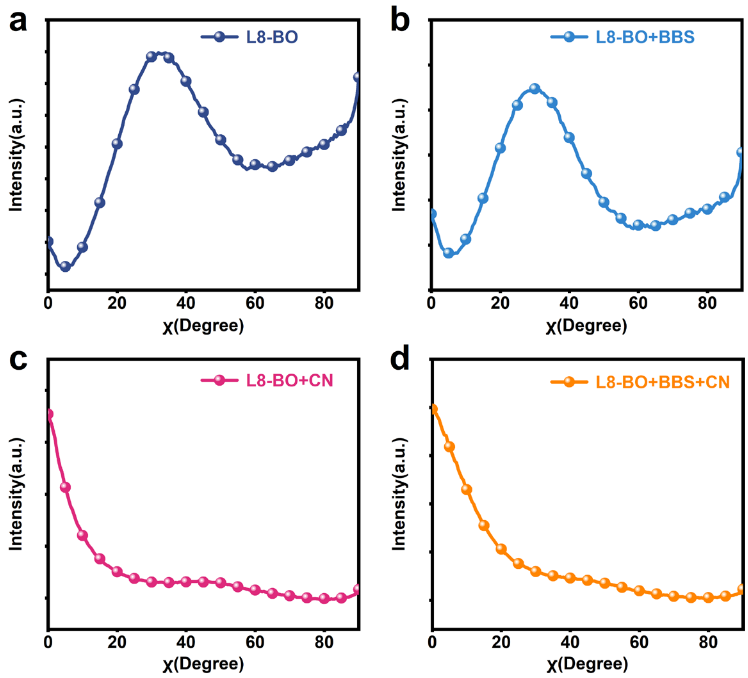

Figure S6. │ The corresponding polar intensity profiles extracted from the (001) diffraction of L8-BO films with and without additives.

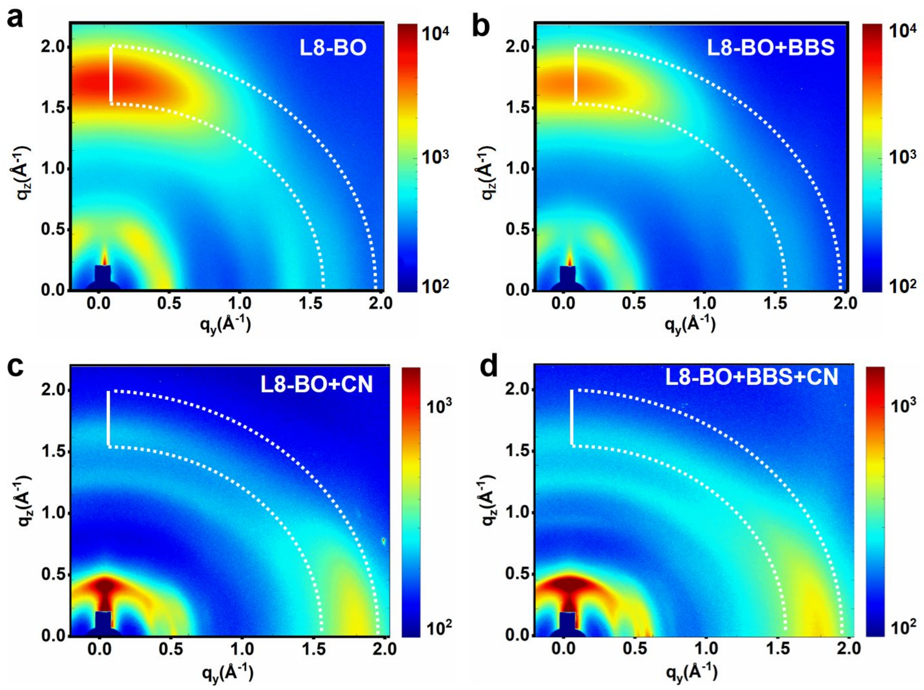

Figure S7. │ 2D-GIWAXS pattern of L8-BO films cast from **a)** DCM, **b)** DCM with BBS, **c)** DCM with CN, and **d)** DCM with BBS+CN.

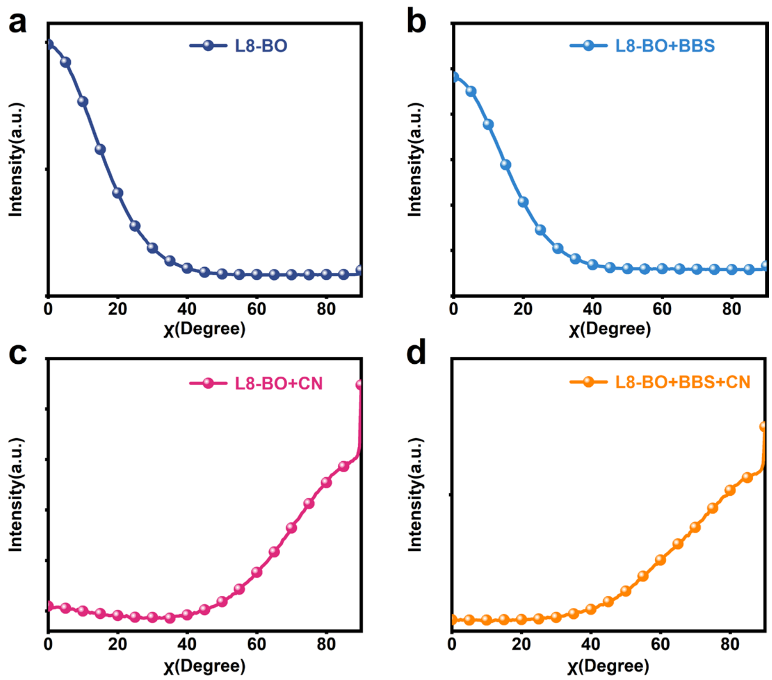

Figure S8. │ The corresponding polar intensity profiles extracted from the (010) diffraction of L8-BO films with and without additives.

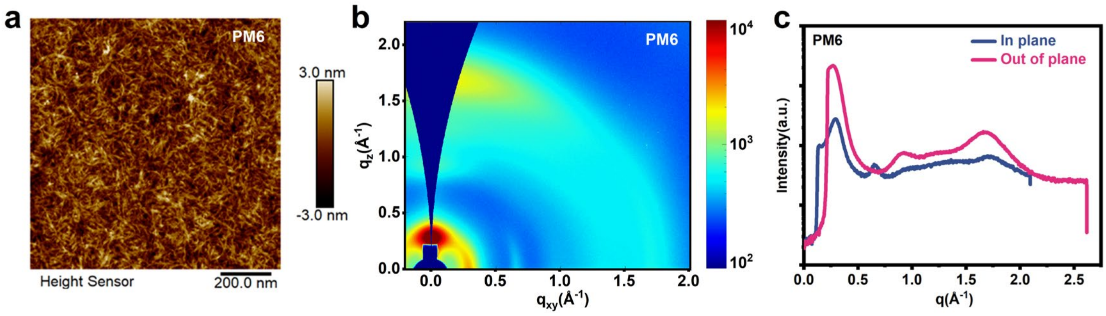

Figure S9. │ a) AFM topography of the PM6 film. **b)** 2D-GIWAXS pattern of the PM6 film. **c)** In-plane (dash lines) and out-of-plane (solid lines) line cuts of the PM6 film.

Table S2 │ In-plane and out-of-plane parameters; peak location, d-spacing, FWHM, and crystal coherence length (CCL) extracted from the 2D GIWAXS of the PM6 film.

Materials	Peak	Peak location ($Å^{-1}$)	d-space (Å)	FWHM ($Å^{-1}$)	CCL (Å)
PM6	(010)	1.67	3.76	0.32	17.56

5. The surface energy of L8-BO films changed with additives

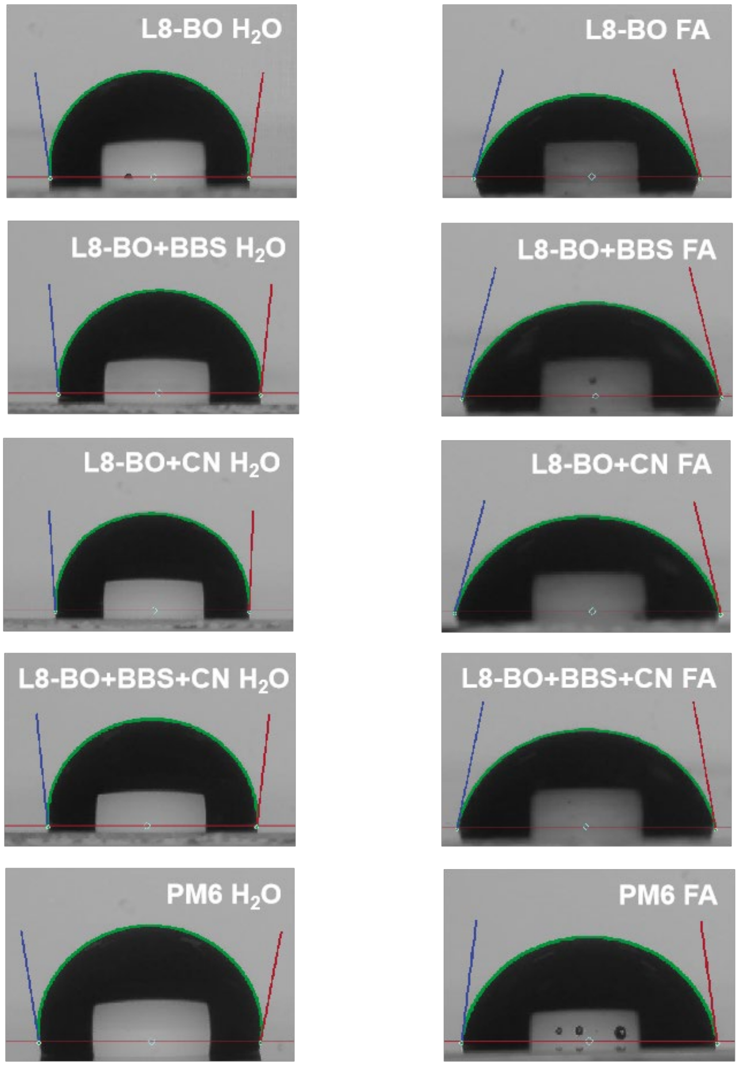

Figure S10. | The contact angles of films without additive treatment.

Table S3 | Parameters of films obtained by contact angle.

L8-BO	H_2O (deg)		Average (deg)	FA (deg)		Average (deg)	Surface free energy (mJ/cm^2)
As-cast	95.91	96.02	95.97	74.83	75.89	75.36	25.31
CN	93.54	92.11	92.83	75.1	76.7	75.90	23.25
BBS	94.89	95.83	95.36	75.59	76.04	75.82	24.46
BBS+CN	95.93	96.36	96.15	78.28	80.12	79.20	21.50
PM6	99.13	100.62	99.88	83.31	82.58	82.95	19.60

6. Evidences of the bilayer active layer

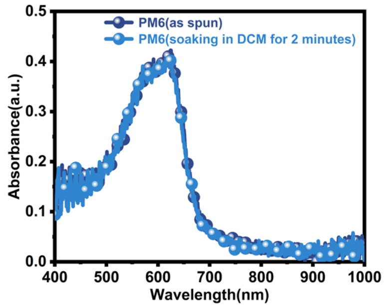

Figure S11. | The immersion video of PM6 film in DCM and the absorption spectra before and after immersion.

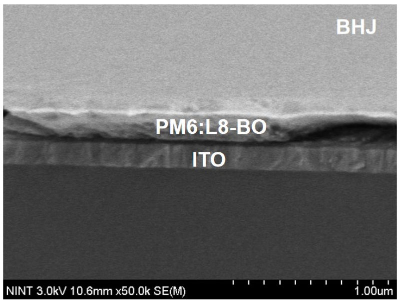

Figure S12. | SEM images of BHJ films based on PM6:L8-BO

7. Optimization processes of bilayer OSCs

Table S4 | Photovoltaic performance of the bilayer OSCs based on PM6/L8-BO changed with PM6 concentration under simulated AM1.5G illumination (100 mW cm^{-2}). Values are averaged by ten devices.

Concentration (mg/mL)	V_{OC} (mV)	J_{SC} (mA/cm^2)	FF (%)	PCE (%)
6/10	913	23.22	75.88	16.09
	(911±2)	(22.42±0.72)	(75.83±1.08)	(15.50±0.65)
8/10	917	26.45	72.97	17.70
	(915±3)	(26.10±0.30)	(72.88±0.26)	(17.40±0.18)
10/10	907	27.53	69.93	17.46
	(907±2)	(26.34±0.66)	(69.67±0.70)	(16.65±0.40)
12/10	907	26.73	64.73	15.70
	(909±3)	(25.08±1.15)	(64.94±0.44)	(14.81±0.69)

Figure S5. Photovoltaic performance of the bilayer OSCs based on PM6/L8-BO changed with L8-BO concentration under simulated AM1.5G illumination (100 mW cm^{-2}). Values are averaged by ten devices.

Concentration (mg/mL)	V_{OC} (mV)	J_{SC} (mA/cm^2)	FF (%)	PCE (%)
8/8	914	26.51	71.71	17.37
	(914±3)	(25.72±0.96)	(72.14±1.34)	(16.95±0.51)
8/10	917	26.45	72.97	17.70
	(915±3)	(26.10±0.30)	(72.88±0.26)	(17.40±0.18)
8/12	905	26.77	72.09	17.46
	(904±1)	(25.76±1.22)	(71.61±1.11)	(16.69±0.78)
8/14	908	25.99	72.41	17.07
	(908±2)	(25.71±0.86)	(71.56±0.44)	(16.62±0.51)

Figure S6. Photovoltaic performance of the bilayer OSCs based on PM6/L8-BO changed with BBS concentration under simulated AM1.5G illumination (100 mW cm^{-2}). Values are averaged by ten devices.

Concentration (mg/mL)	V_{OC} (mV)	J_{SC} (mA/cm^2)	FF (%)	PCE (%)
0	917 (915±3)	26.45 (26.10±0.30)	72.97 (73.01±1.11)	17.70 (17.40±0.18)
0.5	917 (918±3)	27.15 (26.40±0.77)	72.37 (71.76±0.44)	18.01 (17.40±0.60)
1	924 (921±4)	26.98 (26.02±0.67)	72.60 (73.01±1.11)	18.10 (17.50±0.38)
2	929 (927±2)	25.97 (25.09±0.61)	69.03 (69.67±1.14)	16.65 (16.20±0.29)
3	924 (927±3)	25.55 (24.92±1.04)	66.75 (65.52±0.91)	15.75 (15.12±0.60)

Figure S7. Photovoltaic performance of the bilayer OSCs based on PM6/L8-BO changed with CN concentration under simulated AM1.5G illumination (100 mW cm-2). Values are averaged by ten devices.

Volume Fraction (%)	V_{OC} (mV)	J_{SC} (mA/cm^2)	FF (%)	PCE (%)
0	917 (915±3)	26.45 (26.10±0.30)	72.97 (73.01±1.11)	17.70 (17.40±0.18)
0.2	904 (906±3)	26.77 (25.92±0.59)	75.29 (75.82±0.88)	18.21 (17.80±0.30)
0.5	889 (893±4)	27.10 (26.96±0.32)	77.06 (76.38±0.68)	18.56 (18.39±0.17)
1	897 (901±6)	25.87 (25.39±0.58)	76.39 (75.65±1.64)	17.73 (17.17±0.63)
2	886 (877±7)	7.87 (7.36±0.29)	54.62 (54.63±2.00)	3.81 (3.52±0.22)

8. J-V measurements of PM6:L8-BO BHJ devices with and without additives

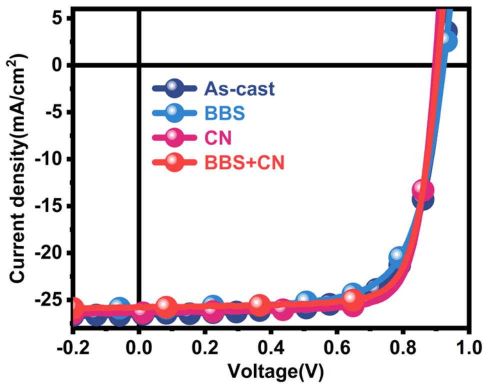

Figure S13. | J-V curves of PM6:L8-BO BHJ devices with or without additives.

Table S8. Photovoltaic performance of the optimized BHJ OSCs based on PM6/L8-BO with or without additives under simulated AM1.5G illumination (100 mW cm^{-2}). Values are averaged by 10 devices.

Materials	V_{OC} (mV)	J_{SC} (mA/cm^2)	FF (%)	PCE (%)
PM6/L8-BO	921 917±7	26.5 25.9±0.5	70.5 70.1±0.4	17.3 16.6±0.4
PM6/L8-BO(BBS)	923 921±2	25.9 25.3±0.6	70.1 69.3±0.7	16.7 16.2±0.3
PM6/L8-BO(CN)	897 897±5	26.4 26.4±0.2	78.0 77.3±0.6	18.5 18.3±0.1
PM6/L8-BO(BBS+CN)	905 893±9	25.8 25.7±0.6	76.4 75.6±1.0	17.8 17.3±0.3

9. EQE of PM6/L8-BO bilayer OSCs changed with additives

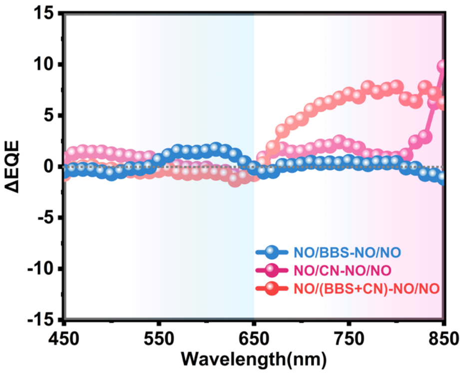

Figure S14. | EQE spectra difference of PM6/L8-BO with and without additives.

10. Dark J-V measurements of bilayer OSCs based on PM6/L8-BO with and without additives

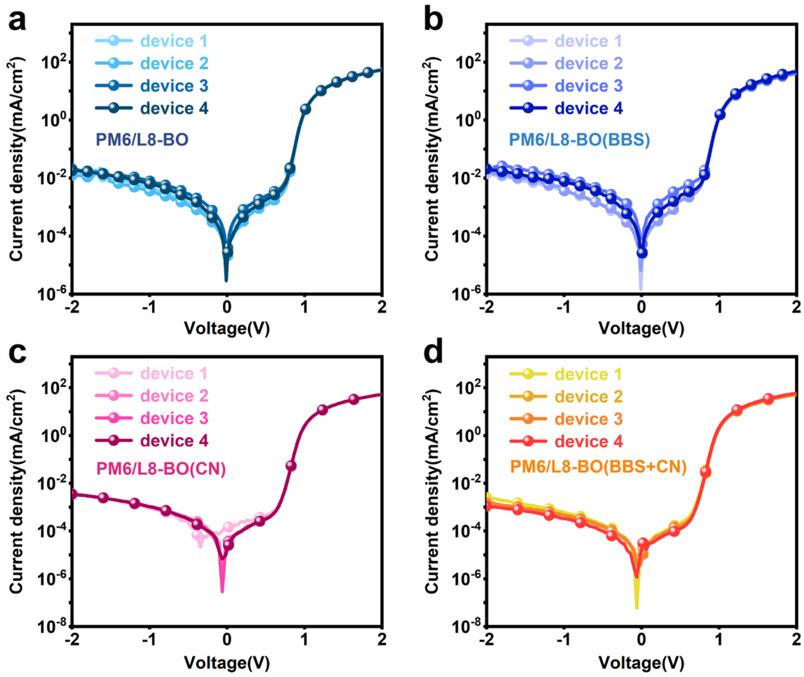

Figure. S15 | Dark J-V curves of PM6/L8-BO bilayer OSCs with and without additives.

11. TPC measurements of bilayer OSCs based on PM6/L8-BO

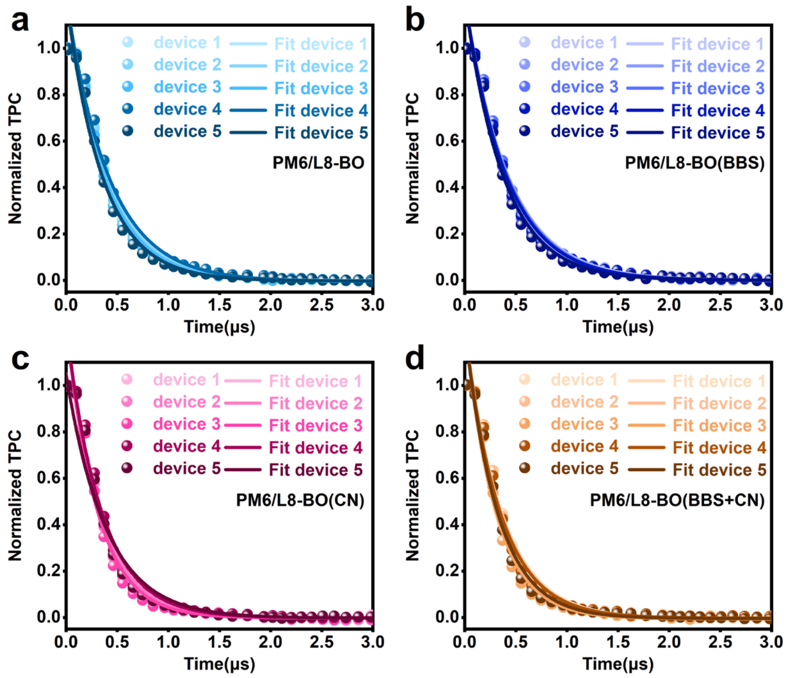

Figure. S16 | TPC curves of PM6/L8-BO bilayer OSCs with and without additives.

Table. S9 | Charge extraction time fitted by TPC measurements of bilayer devices based on PM6/L8-BO with and without additives.

Condition	Device 1	Device 2	Device 3	Device 4	Device 5
As-cast	0.39 μs	0.39 μs	0.37 μs	0.41 μs	0.36 μs
BBS	0.43 μs	0.39 μs	0.42 μs	0.41 μs	0.38 μs
CN	0.33 μs	0.33 μs	0.31 μs	0.35 μs	0.34 μs
BBS+CN	0.36 μs	0.35 μs	0.30 μs	0.34 μs	0.31 μs

12. TPV measurements of bilayer OSCs based on PM6/L8-BO

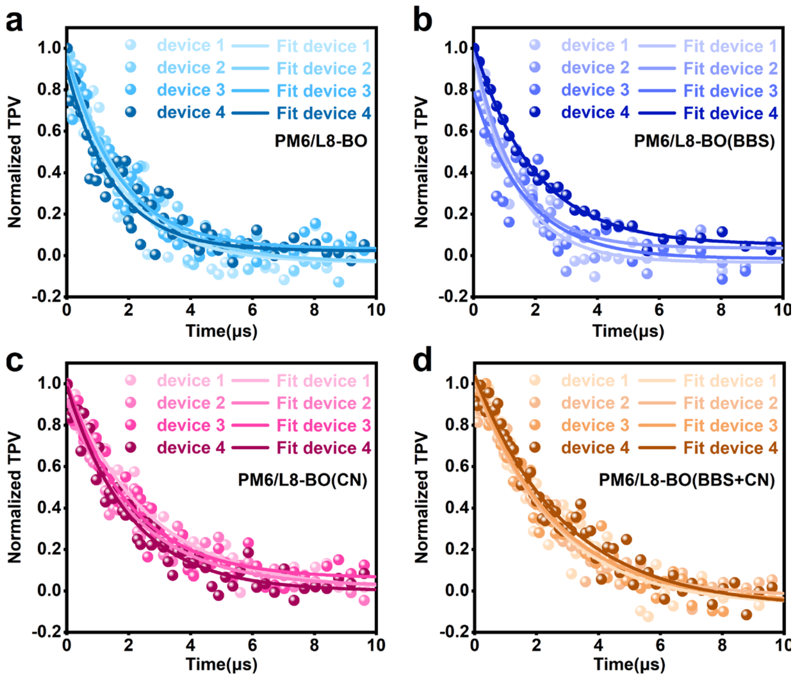

Figure. S17 | TPV curves of PM6/L8-BO bilayer OSCs with and without additives.

Table. S10 | Carrier lifetime fitted by TPV measurements of bilayer OSCs based on PM6/L8-BO with and without additives.

Condition	Device 1	Device 2	Device 3	Device 4
As-cast	1.78 μs	1.93 μs	1.69 μs	1.51 μs
BBS	1.37 μs	1.35 μs	1.66 μs	1.96 μs
CN	2.67 μs	2.23 μs	2.07 μs	2.03 μs
BBS+CN	2.45 μs	2.38 μs	2.56 μs	2.89 μs

13. J-V curves of bilayer OSCs based on PM6/L8-BO

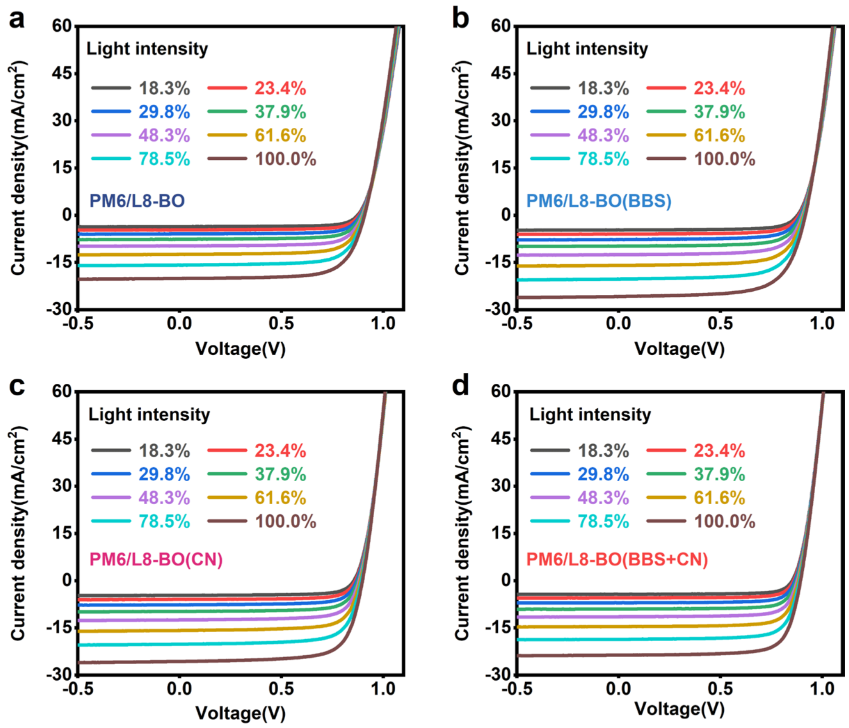

Figure. S18 │ J-V curves of PM6/L8-BO bilayer OSCs with and without additives changed with light intensity.

14. DoS calculation

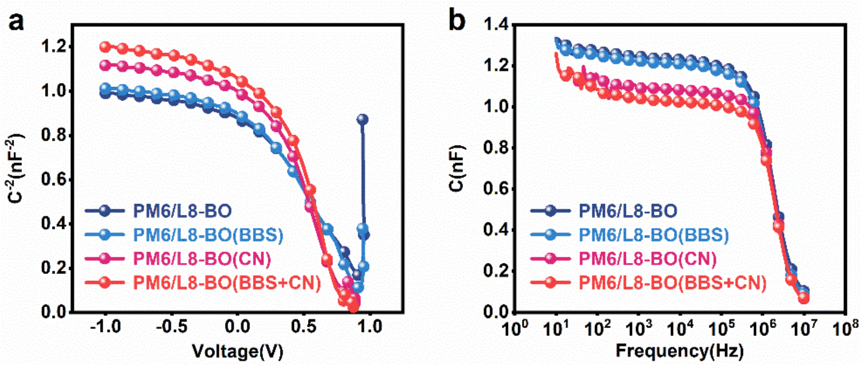

Figure. S19 │ a) Mott-schottky spectra of devices based on PM6/L8-BO with and without additives. b) Capacitance-frequency spectra of devices based on PM6/L8-BO with and without additives.

The density of the state of trap distributions was performed through measurement of capacitance spectroscopy in a dark environment. In which, we applied capacitance-voltage (C-V) measurements under a frequency of 100 kHz at a different applied voltage from -1V to 1.2V (**Figure S16a**), and in the capacitance-frequency (C-f) measurement a varied frequency from 10 MHz to 10 Hz were used (**Figure S16b**).
The demarcation energy E_ω and modulation frequency ω are described as:

$$\omega = \omega_0 \exp(-\frac{\Delta E}{k_B T}) \tag{1}$$

with the solution of:

$$E_\omega = k_B T ln(\frac{\omega_0}{\omega}) \tag{2}$$

The trap density at energy DoS (E_ω) can be acquired as:

$$\mathrm{DoS}(E_\omega) = -\frac{V_{bi}}{qW}\frac{dC}{d\omega}\frac{\omega}{k_B T} \tag{3}$$

Where $\omega_0 = 2\pi\nu_0$ ($\nu_0 = 10^{12}$ s^{-1}) is called the attempt-to-escape frequency, W is the depletion width, $\frac{dC}{d\omega}$ is the derivative of each point in the capacitance with respect of AC frequency. [3,4]

Table. S11 | Energetic disorder fitted by capacitance−voltage and capacitance−frequency measurements of bilayer OSCs based on PM6/L8-BO with and without additives.

Condition	**FWHM (meV)**	**E_0 (meV)**	**n_t ($\times 10^{16}/cm^3$)**	**σ (meV)**
As-cast	49.8	29.6	1.72	22.8
BBS	47.9	29.7	1.62	22.2
CN	44.4	29.3	1.28	19.8
BBS+CN	44.2	29.3	1.17	19.8

15. DLTS measurements of bilayer OSCs based on PM6/L8-BO

In this experiment, a method of transient photocurrent was used to the DLTS measurement. [5,6] In there, when a bias of 0V was applied the traps in space charge region were populated, and after a reverse bias of -2.5V used the trap filled can emit the captured charge carriers for heating up to a new bias condition. The carrier emission process is observed as a current transient in the device current signal. By following equation according to experimental data the trapped defect state volume density N_t can be given:

$$j_{te}(t) = \frac{1}{\tau_{te}} \cdot q \cdot d \cdot N_t \cdot exp\left(-\frac{t}{\tau_{te}}\right) \tag{4}$$

Here, j_{te} is trap emission current, τ_{te} is catch-trap emission time constant, q is a single charge amount, d is the thickness of the device.

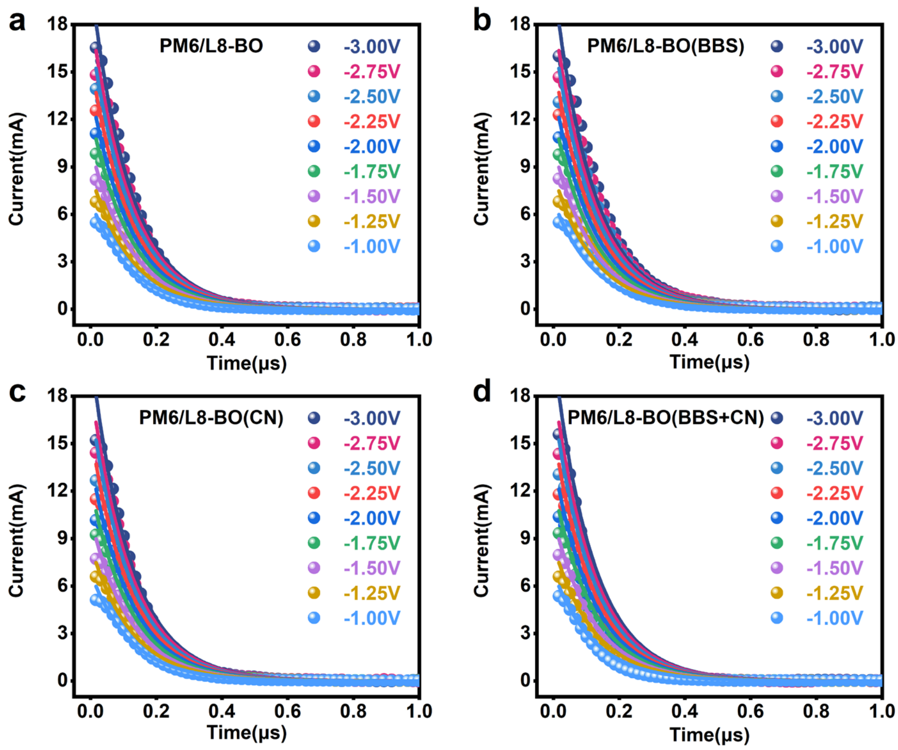

Figure. S20 | Transient photocurrent of bilayer OSCs based on PM6/L8-BO with and without additives changed with applied voltage.

16. AFM measurements of N3 with and without additives

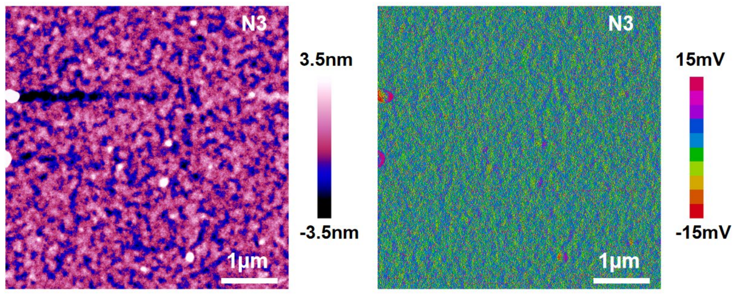

Figure. S21 │**a)** AFM topography of N3 films cast from DCM. **b)** Peak force error topography of N3 films cast from DCM.

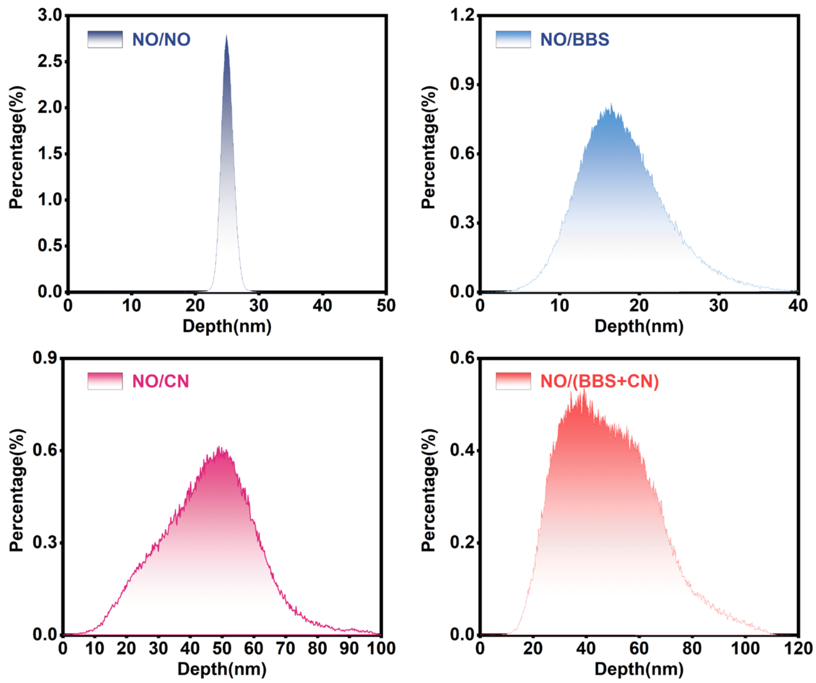

Figure. S22 │ Depth of N3 films changed with additives.

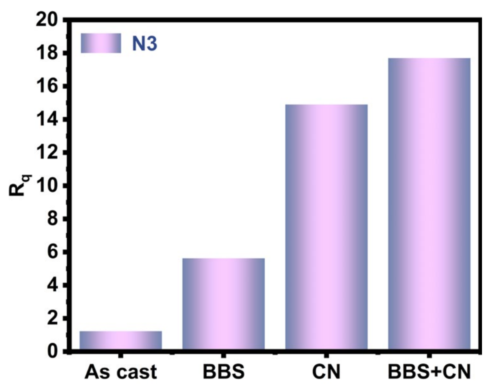

Figure. S23 │ Roughness of N3 films changed with additives.

17. Bimolecular recombination calculation

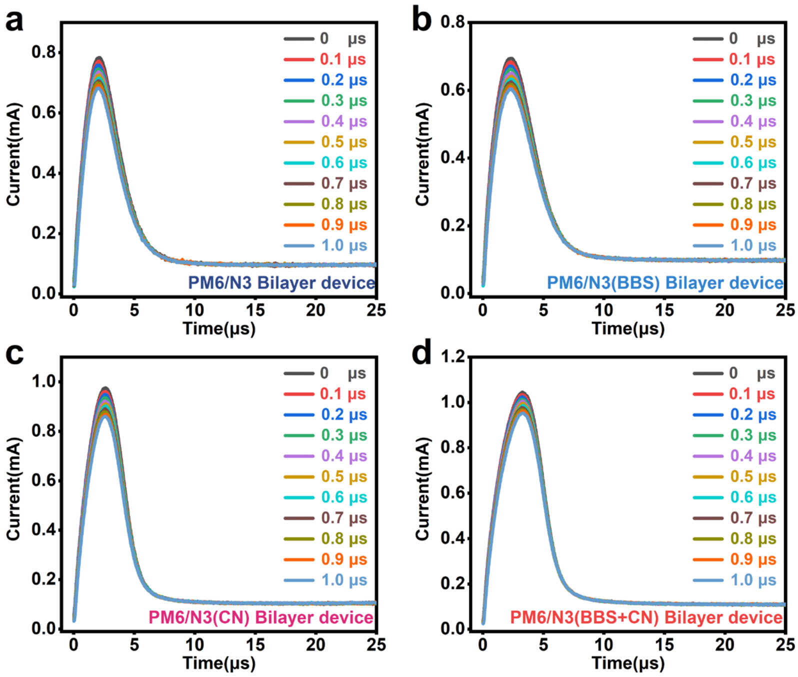

Figure. S24 │ Current versus time of bilayer OSCs based on PM6/N3 with and without additives obtained by photo-CELIV measurements.

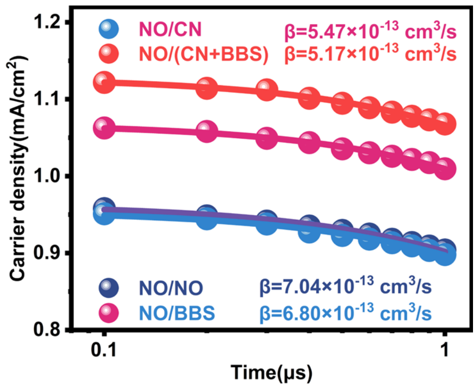

Figure. S25 │ Charge carrier density of bilayer OSCs based on PM6/N3 with and without additives as a function of delay time and the bimolecular recombination fits (solid lines).

18. J-V curves of bilayer OSCs based on PM6/N3

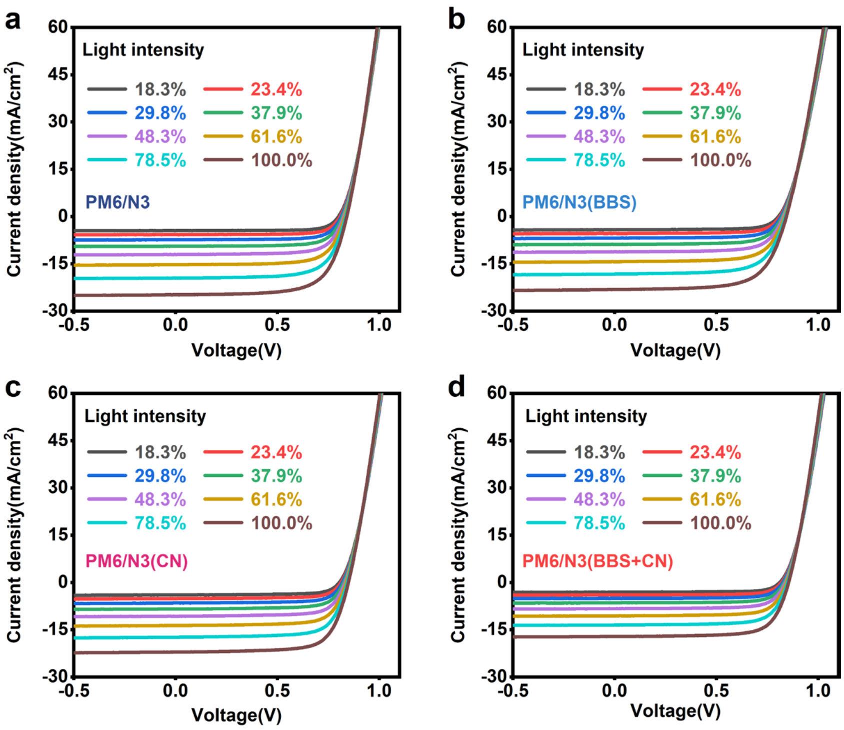

Figure. S26 | J-V curves of PM6/N3 bilayer OSCs with and without additives changed with light intensity.

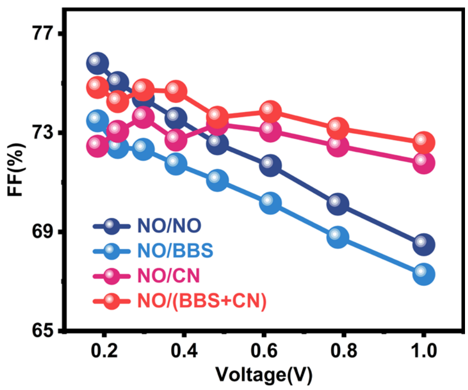

Figure. S27 | The change of FF with voltage of bilayer OSCs based on PM6/N3 with and without additives.

19. DLTS measurements of bilayer OSCs based on PM6/N3

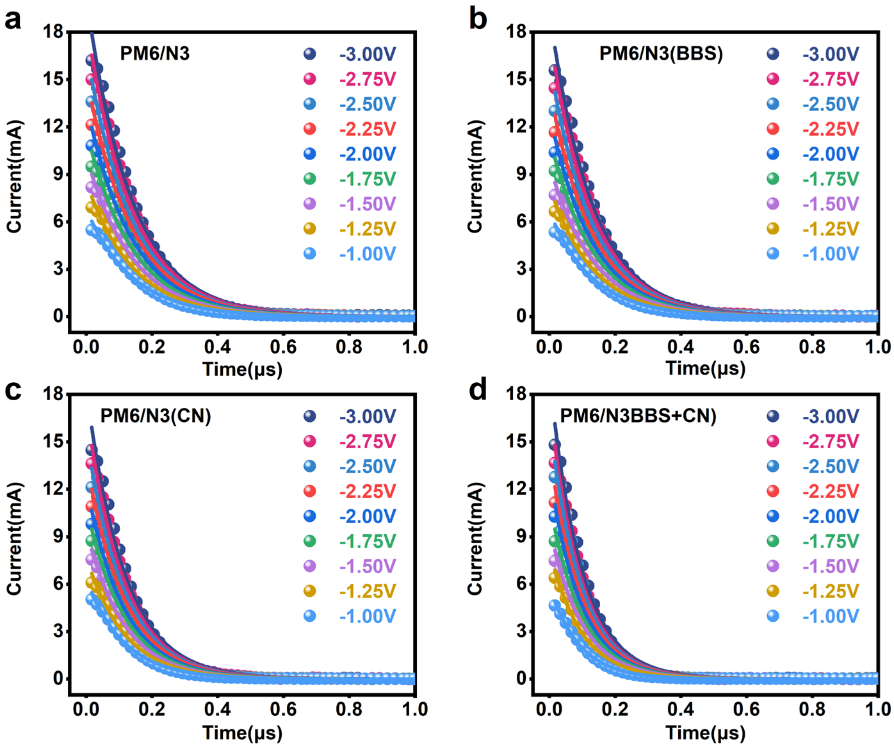

Figure. S28 | Transient photocurrent of bilayer devices based on PM6/N3 with and without additives changed with applied voltage.

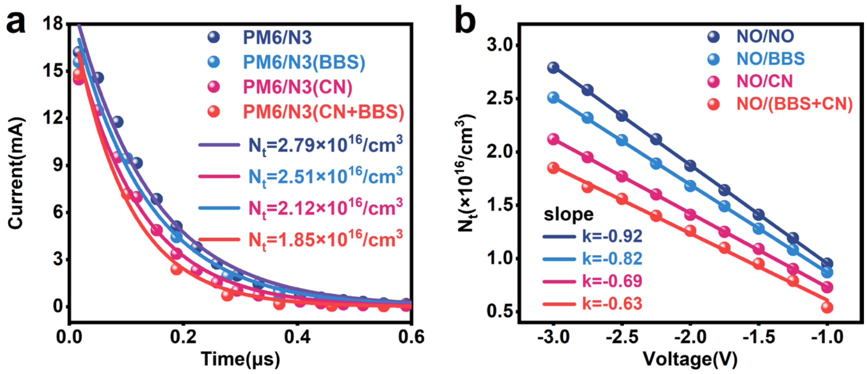

Figure. S29 | The change of DLTS with voltage of bilayer OSCs based on PM6/N3 with and without additives.

20. References

(1) Qin, Y. et al. Low Temperature Aggregation Transitions in N3 and Y6 Acceptors Enable Double-Annealing Method That Yields Hierarchical Morphology and Superior Efficiency in Nonfullerene Organic Solar Cells. *Adv. Funct. Mater. 30,* 2005011 (2020).

(2) Sun, R. et al. A Layer-by-Layer Architecture for Printable Organic Solar Cells Overcoming the Scaling Lag of Module Efficiency. *Joule.* **4,** 407-419 (2020).

(3) Ni, Z. et al. Resolving spatial and energetic distributions of trap states in metal halide perovskite solar cells. *Science.* **367,** 1352–1358 (2020).

(4) Jiang, K. et al. Alkyl chain tuning of small molecule acceptors for efficient organic solar cells. *Joule.* **3,** 3020-3033 (2019).

(5) Bozyigit, D. et al. Deep Level Transient Spectroscopy (DLTS) on Colloidal-Synthesized Nanocrystal Solids. *ACS Appl. Mater. Interfaces.* **5,** 2915−2919 (2013).

(6) Li, R. et al. Self-Structural Healing of Encapsulated Perovskite Microcrystals for Improved Optical and Thermal Stability. *Adv. Mater.* ***33*****,** 2100466 (2021).